IEEE Photonics Journal
An IEEE Photonics Society Publication

Dual-Operation Regime Thulium-Doped Fiber Laser and Its Applications in Cascaded Raman Light and Supercontinuum Generation

Volume 10, Number 1, February 2018

Zhijian Zheng
Deqin Ouyang
Junqing Zhao
Peiguang Yan
Jinzhang Wang
Shenghua Lin
Shuangchen Ruan

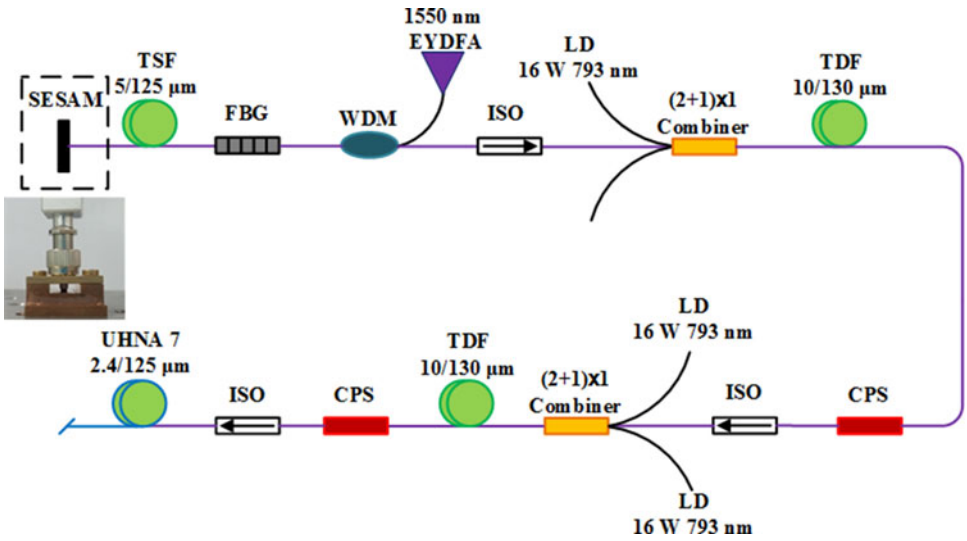

DOI: 10.1109/JPHOT.2018.2794974
1943-0655 © 2018 IEEE

Dual-Operation Regime Thulium-Doped Fiber Laser and Its Applications in Cascaded Raman Light and Supercontinuum Generation

Zhijian Zheng,[1] **Deqin Ouyang**,[1] **Junqing Zhao**,[2] **Peiguang Yan**,[1] **Jinzhang Wang**,[1] **Shenghua Lin**,[1] **and Shuangchen Ruan** [1]

[1]Shenzhen Key Laboratory of Laser Engineering, Key Laboratory of Advanced Optical Precision Manufacturing Technology of Guangdong Higher Education Institutes, College of Optoelectronic Engineering, Shenzhen University, Shenzhen 518060, China
[2]School of Physics and Electronic Engineering, Jiangsu Normal University, Jiangsu 221116, China

DOI:10.1109/JPHOT.2018.2794974

Manuscript received October 20, 2017; revised December 21, 2017; accepted January 15, 2018. Date of publication January 18, 2018; date of current version February 7, 2018. This work was supported in part by the National Natural Science Foundation of China under Grant 61575129 and Grant 61605122, in part by the Guangdong Natural Science Foundation under Grant 2016A030310049, and in part by the Shenzhen Science and Technology Project under Grant KQJSCX20160226194031. Corresponding author: Shuangchen Ruan (e-mail: scruan@szu.edu.cn).

Abstract: We report on a passively mode-locked thulium-doped fiber laser (TDFL) with dual operation regimes and applications in cascaded Raman light and supercontinuum generation. The mode-locking is initiated by using a semiconductor saturable absorber mirror (SESAM) and can operate at both fundamental mode-locking and noise-like twin-pulse regimes. Output power can be scaled up through two-stage amplifications, and then was further fed into a segment of ultrahigh numerical aperture (NA) single-mode fiber with a length of $\sim$30 m. At the fundamental mode-locking regime, two orders of stokes lights can be generated, centered at 2.13 and 2.35 μm, respectively, with a maximum total power of 3.75 W. At the noise-like twin-pulse regime, a near-infrared supercontinuum from 1.93 to 2.46 μm was generated with a maximum average output power of 2.5 W. It is, to the best of our knowledge, the first demonstration of both cascaded Raman light and supercontinuum generation with the same system.

Index Terms: Thulium-doped fiber lasers, supercontinuum generation, Raman, laser amplifiers.

1. Introduction

Mode-locked lasers have attracted significant attentions in the past decades, which have been proved to be very useful in many fields such as spectroscopy [1], [2], medical applications [3], [4], material processing [5], [6], nonlinear optics [7], [8], and so on. Active and passive methods are two common ways to obtain mode-locked pulses in a laser. For passive mode-locking, different kinds of saturable absorbers (SAs), such as graphene [9]–[11], carbon nanotubes (CNTs) [12]–[14], topological insulators (TIs) [15]–[18], semiconductor saturable absorber mirrors (SESAMs)

[19]–[21], and even artificial saturable absorbers such as nonlinear polarization rotation (NPR) [22]–[24] can be candidates.

Under the interaction of nonlinearity and dispersion, passively mode-locked fiber lasers might lead to different evolution phenomena. Passively mode-locked fiber lasers with various operating states have been widely investigated both theoretically and experimentally. In 2000, Komarov *et al.* theoretically analyzed the multi-stable operation of laser passive mode-locking by complex Ginzburg-Landau equation (CGLE), and found that nonlinear refractive index plays an important role in multi-stable operation [25]. Later, in 2007, Schreiber *et al.* showed the pulse evolution in mode-locked fiber laser by solving the nonlinear Schrodinger equation (NLSE) and revealed that different solutions can be obtained in the transient region between mode-locking regimes [26]. Experimentally, Wang *et al.* demonstrated a nonlinear polarization evolution (NPE) based all-fiber mode-locked thulium-doped fiber laser (TDFL) ring oscillator [27]. The oscillator could operate at both solitary and noise-like pulse regimes, which can be switched by changing the pump power. In 2014, Li *et al.* reported an all-fiber mode-locked double-clad TDFL with a nonlinear optical loop mirror (NOLM) structure and large net anomalous dispersion for the first time [28]. Stable solitary and noise-like mode-locked pulses were both observed at all-anomalous-dispersion regime by carefully adjusting the pump power and polarization state. Later, in 2016, Sobon *et al.* obtained ultra-broadband dissipative soliton and noise-like pulse from a normal dispersion NPE based mode-locked TDFL [29]. Very recently, Kwon *et al.* theoretically studied the multi-pulse dynamics in an anomalous dispersion fiber ring oscillator [30], where they showed that the cavity could operate in as many as five different mode-locked regimes, depending on the saturation power of the SA and characteristic of the cavity such as nonlinearity and dispersion. All the previous works were focus on the characteristics of the mode-locked oscillator. However, to our best knowledge, optical amplification characteristics of the TDFL which could operate in multi-operation regime have not been explored.

In this work, we report on a SESAM based mode-locked TDFL system, which can operate at both fundamental mode-locking and noise-like twin-pulse regimes. A typical two-stage power amplifier is utilized to boost the output power to pump a segment of highly Ge-doped ultra-high numerical aperture (UHNA) fiber. Cascaded Raman light up to 2.35 μm and supercontinuum covered from 1.93 to 2.46 μm can be finally generated with two operation regimes, respectively.

2. Experimental Setup and Results

2.1 Experimental Setup

The schematic setup of the system is shown in Fig. 1, which is constructed with a MOPA structure and an additional segment of UHNA fiber. The oscillator is constructed with a typical linear configuration which contains a semiconductor saturable absorber mirror (SESAM), a segment of gain fiber and a fiber Bragg grating (FBG). The SESAM has a modulation depth of 20% and a relaxation time of 10 ps. The transmittance at 1.95 μm and 3 dB bandwidth of the FBG are 15% and 0.9 nm, respectively. The inset of Fig. 1 gives the actual SESAM sandwiched between a fiber connector and a passive heat sink. An Er/Yb co-doped fiber amplifier (EYDFA) is used as the pump source and connected with a wavelength division multiplexing (WDM). A segment of highly thulium-doped single-mode single-clad fiber (TSF) is used as the gain medium. The TSF is 9 cm long with a high core absorption coefficient of 340 dB/m at 1.56 μm. The core/cladding diameter and the corresponding core NA of the TSF are 5/125 μm and 0.24, respectively. An optical isolator (ISO) is used to prevent unwanted reverse transmission light into the oscillator that may induce parasitic lasing.

The fiber preamplifier contains a $(2 + 1) \times 1$ pump combiner, a segment of thulium-doped single-mode double-clad fiber (TDF), a home-made cladding power stripper (CPS) and an ISO. The $(2 + 1) \times 1$ pump combiner is used to launch the pump light into the TDF from a 16 W, 793 nm, fiber-pigtailed multi-mode laser diode (LD). The TDF is 3 m long with cladding absorption of 3 dB/m at 793 nm, core/cladding diameter of 10/130 μm, and core NA of 0.15, respectively. The home-made CPS is used to remove the residual pump power from the cladding, which is a necessary protection for the following ISO. In the fiber amplifier, an effective CPS is usually used to strip the

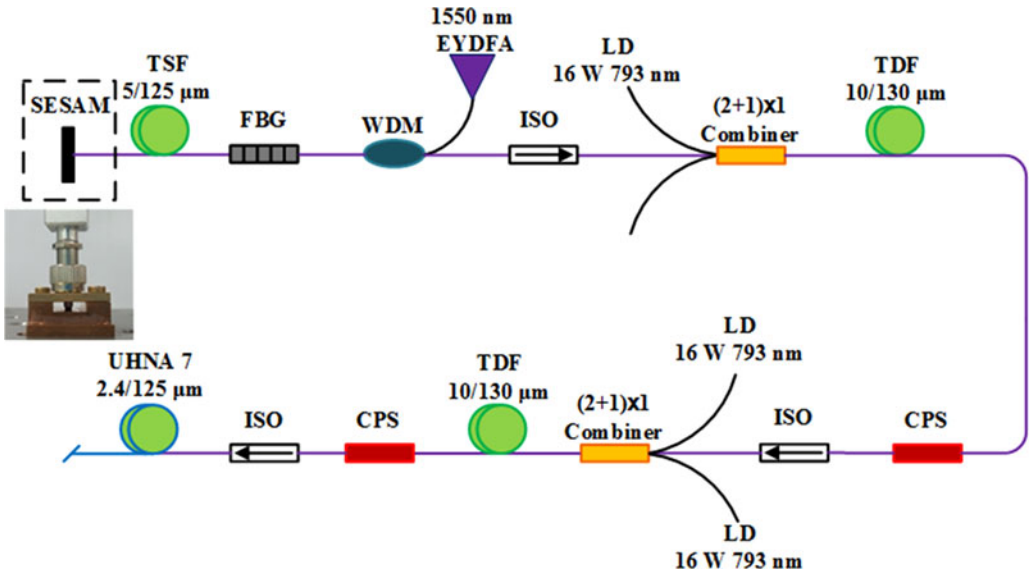

Fig. 1. Schematically experimental setup. SESAM: semiconductor saturable absorber mirror; TSF: thulium-doped single-mode single-clad fiber; FBG: fiber Bragg grating; WDM: wavelength division multiplexing; ISO: isolator; TDF: thulium-doped single-mode double-clad fiber; CPS: cladding power stripper. Inset: SESAM sandwiched between a fiber connector and a passive heat sink.

unabsorbed pump light for protecting the rear optical fiber devices. During our experiment, the CPS is fabricated with a segment of SMF-28. Firstly, we remove about 3 cm long protective polymer in the middle of the passive fiber and clean the striped-fiber. Secondly, we fix the striped-fiber onto a 5 cm long sapphire with high-refractive-index UV glue which is cured by a handheld UV lamp. The final power amplifier has a similar structure as the preamplifier except that it has a 4 m long TDF and two 16 W, 793 nm LDs.

Following the thulium-doped fiber amplifier (TDFA) is a 30 m long UHNA single-mode fiber (UHNA 7), which is a highly Ge-doped step-index fiber. The core/cladding diameter and core NA of the UHNA 7 fiber are 2.4/125 μm and 0.41, respectively. The UHNA 7 fiber is directly fusion spliced to the output port of the ISO. The fusion splicing loss is about 0.7 dB, which is mainly caused by the large MFD mismatch.

In the experiment, the pulse train of the oscillator is measured via a high-speed InGaAs photodetector (EOT, ET-5000) combined with a 1-GHz bandwidth digital oscilloscope (Tektronix, DPO 7104C). An autocorrelator (APE, pulseCheck USB) is used to measure the autocorrelation (AC) trace of the pulse. The optical spectrum of the oscillator is measured by an optical spectrum analyzer (YOKOGAWA, AQ6375B). The generated Raman and supercontinuum spectra are characterized by using a Fourier transform IR spectroscopy (Bruker, Tensor 27).

2.2 Fundamental Mode-Locking Regime and Cascaded Raman Light

The emission characteristics of the oscillator are shown in Fig. 2. Self-starting mode-locked pulses were achieved when the launched pump power was increased to 744 mW. The high core absorption gain fiber of the oscillator is responsible for the relative high threshold power. Fig. 2(a) shows the pulse train of the fundamentally mode-locked fiber laser. The repetition rate is 35.06 MHz, defined by the total cavity length. Fig. 2(b) plots the RF spectrum at the fundamental repetition rate by using a 100-Hz resolution bandwidth, which gives a signal-to-noise ratio (SNR) of $\sim$65 dB. Fig. 2(c) shows the RF distribution with 1 GHz span. We have also measured the AC trace of the pulse. Due to the low power of the oscillator and the low sensitivity of our autocorrelator, the AC trace is measured at the output port of the fiber preamplifier. Fig. 2(d) gives the AC trace of the pulse. The measured FWHM of the AC trace is 34.3 ps. Assuming a sech2 profile, the pulse duration is 22.2 ps. Fig. 2(e) shows the spectrum of the fiber laser, with a central wavelength of 1950.4 nm and

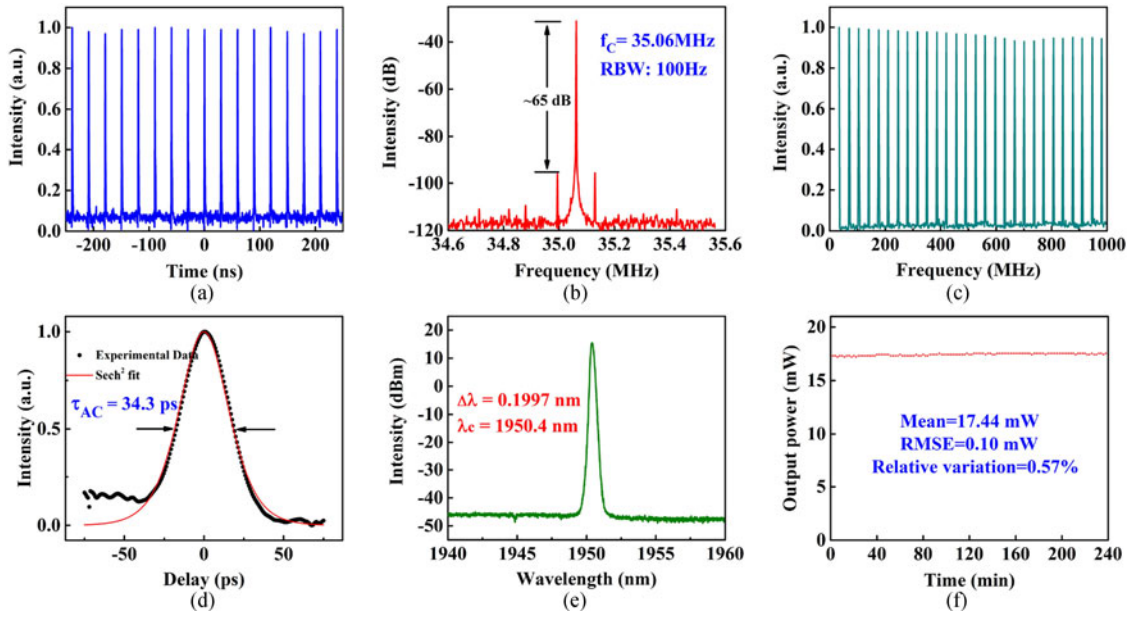

Fig. 2. Oscillator under fundamental mode-locked operation: (a) pulse train; (b) RF spectrum at the fundamental repetition rate; (c) RF spectrum with 1 GHz span; (d) AC trace of the pulse; (e) output spectrum; (f) power stability.

3 dB bandwidth of ~0.1997 nm. In order to test the long-term stability of the oscillator, we have also further measured the output power pumped at 1 W for 4 hours, as shown in Fig. 2(f). The mean value and root-mean-square error (RMSE) of the power was calculated to be 17.44 and 0.10 mW, respectively. The corresponding relative variation is only 0.57%, which can be useful to quantify the power stability of the oscillator.

With the help of the following two-stage amplifiers, the output power can be boosted up to ten-watt-level, while no obvious spectral broadening is observed. After propagating through the UHNA 7 fiber, as shown in Fig. 3, cascaded Raman spectra gradually appeared with the increase of the incident pump power. The measured cascaded Raman peaks are centered at 2.13 and 2.35 μm, corresponding to the 1st and the 2nd order Stokes light, respectively. With the maximum incident pump power at 1.95 μm, the output power is 3.75 W, which is much higher than the previous reports [31], [32]. It can be observed that with the increase of output power, more and more energy is transferred into the Raman wavelength. However, due to the very high loss of the UHNA 7 fiber at the wavelength >2.5 μm, it is difficult to obtain the 3rd Stokes Raman light. For achieving higher Stokes generation, higher peak power pump laser is required [32]. A Raman spectrometer (Horiba, LabRAM HR evolution) is also used to measure the Raman shift of the UHNA 7 fiber. The measured Raman shift constant Δw is about 430 cm^{-1}, as shown in the inset of Fig. 3. In the Raman laser, the amplified Stokes light can generate the next order Stokes light in succession [31]. According to the formula $\frac{1}{\lambda_p} - \frac{1}{\lambda_s} = \Delta w$, we can calculate the center wavelength of the cascaded Raman light, where λ_p is the pump wavelength and λ_s is the corresponding Stokes wavelength, respectively. When the pump wavelength is set at 1.95 μm, the calculated 1st and 2nd order Stokes Raman wavelengths are 2.128 and 2.346 μm, respectively. The measured Stokes Raman wavelengths agree well with that the calculations.

Fig. 4 depicts the different output power from the TDFA and the UHNA 7 fiber. The output power of the TDFA was measured after the ISO. We can see that the TDFA output increases almost linearly with the rise of incident pump power. The corresponding slope efficiency is 33%. The maximum output power of the TDFA is 9.16 W at the incident pump power of 28.7 W, limited by the available pump power. The corresponding peak power is estimated to 11.7 kW. However, with the growth of pump power, the slope efficiency of the output power of UHNA 7 fiber dramatically decreases from 18% to 8%. More and more energy is dissipated into heat due to the fiber attenuation at

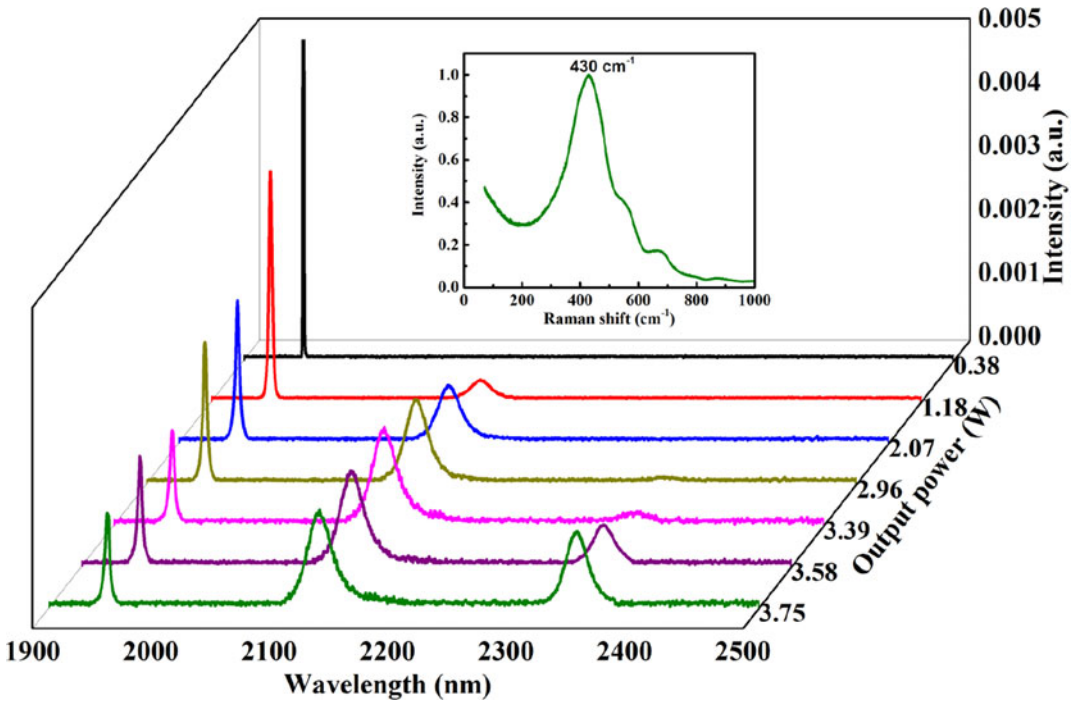

Fig. 3. Output spectra from the UHNA 7 fiber at different output power. Inset: Measured Raman shift of the UHNA 7 fiber.

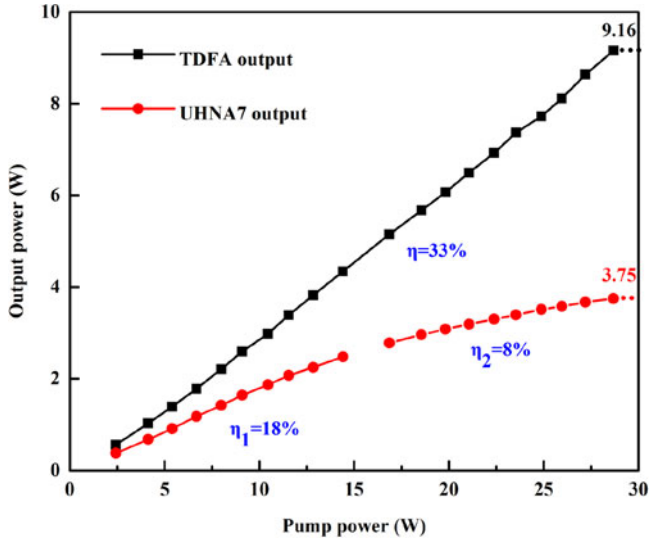

Fig. 4. Output power of the TDFA and the UHNA 7 fiber versus the incident pump power.

the long-wavelength region. The conversion efficiency can be optimized by changing the length of the nonlinear fiber. And one can utilize a longer wavelength laser pump source to obtain longer cascaded Raman light [32].

2.3 Noise-Like Twin-Pulse Regime and Supercontinuum Generation

We can also obtain the noise-like twin-pulse regime through careful adjustment of the SESAM and fiber connector. During the adjustment, the intra-cavity polarization states and the energy density

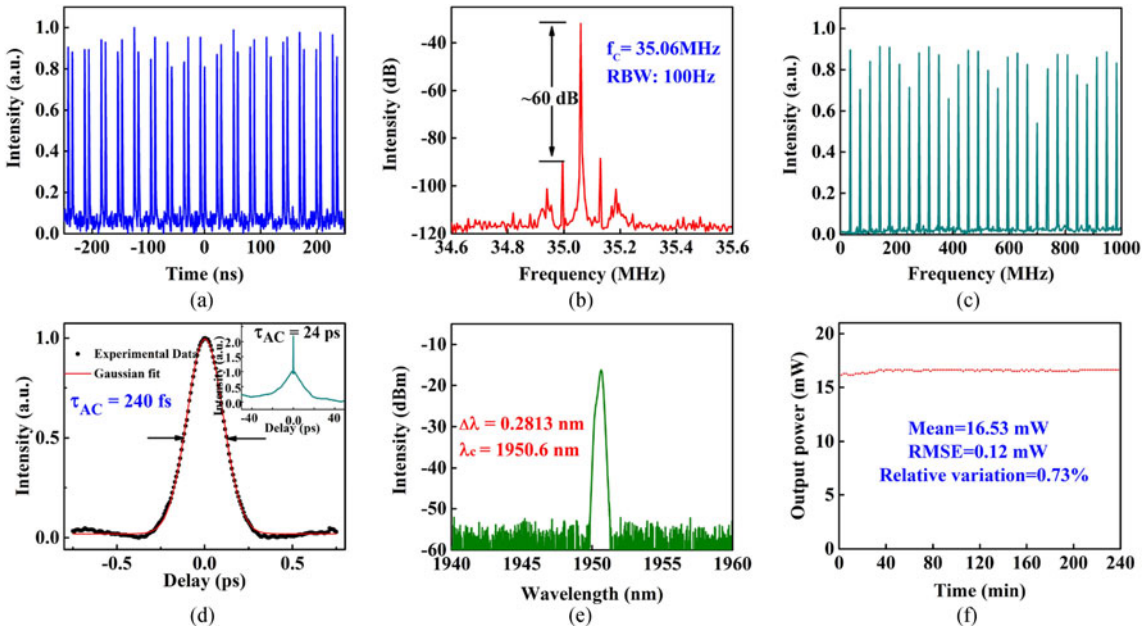

Fig. 5. Oscillator under noise-like twin-pulse operation: (a) pulse train; (b) RF spectrum at the fundamental repetition rate; (c) RF spectrum with 1 GHz span; (d) AC trace of the pulse; (e) output spectrum; (f) power stability.

on SESAM could be changed. Fig. 5 plots the output characteristics of the noise-like twin-pulse regime. From the pulse train plotted in the Fig. 5(a), it can be seen that the pulse is less stable than that of the previously mode-locked operation. The RF spectrum of output pulses at the fundamental repetition rate with a SNR of ~60 dB is shown in Fig. 5(b), which also verifies the noise-like twin-pulse regime is less stable than the fundamental mode-locking regime. The repetition rate for the output pulse train is 35.06 MHz, which is still well matched with the total cavity length. Fig. 5(c) gives the RF spectrum for a 1 GHz span. It also indicates that the laser is not operating in the second-order harmonic mode-locking, even though the pulse number is doubled. Fig. 5(d) shows the AC trace of the noise-like pulse. The AC trace is also measured at the output port of the fiber preamplifier. As the inset of the Fig. 5(d) shows, the AC trace has a fs-level narrow peak located in a ps-level wide pedestal, which is a key signature of a noise-like pulse. The fluctuations of the wide span RF spectrum confirm that the noise-like pulse is temporally fluctuant [32]. The FWHM of the peak and pedestal are measured to be 240 fs and 24 ps. Assuming a Gaussian profile, the narrow peak and pedestal has duration of 170 fs and 17 ps, respectively. Fig. 5(e) gives the spectrum of the oscillator, with a central wavelength of 1950.6 nm. Due to the narrow bandwidth of the FBG, the 3 dB bandwidth of the spectrum is only 0.2813 nm, little wider than the fundamental mode-locking regime. We have also measured the long-term stability of the oscillator at 1 W pump power for 4 hours, as shown in Fig. 5(f). The calculated mean output power and RMSE was 16.53 and 0.12 mW, with a relative variation of 0.73%.

The noise-like pulse is further amplified in the same system. In the process of amplification, the fs-level narrow peak will induce spectrum broadening and reduce the slope efficiency. When the incident pump power is 16.9 W, the corresponding output power of TDFA after the ISO is only 4 W. Because the noise-like pulse consists of stochastic fs-level pulses, the corresponding peak power is also stochastic. Further increase the incident pump power, the output power of the TDFA grows more and more slowly. As Fig. 6 shows, due to the high peak power, the output spectrum of the TDFA is obviously broadening up to 2.17 μm, while at fundamental mode-locking regime no obvious spectral broadening is observed.

Fig. 7 gives the output spectra of the UNHA 7 fiber at an average output power of 0.84, 1.40, 1.83, 2.20 and 2.50 W, respectively. It can be clearly seen that as the increasing of the output power, the

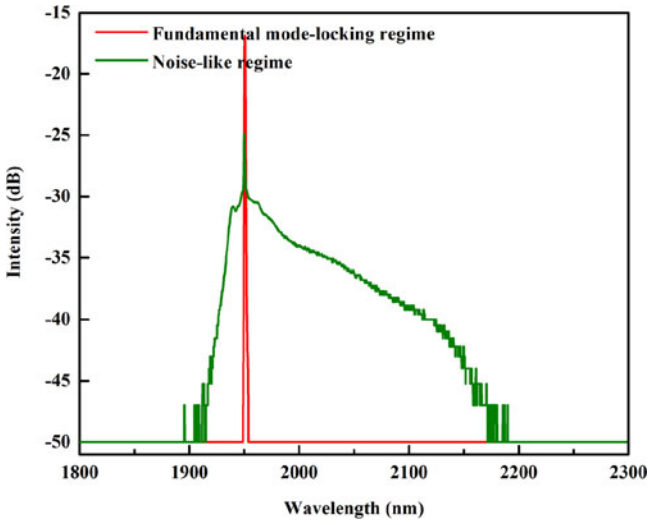

Fig. 6. Output spectra of the TDFA.

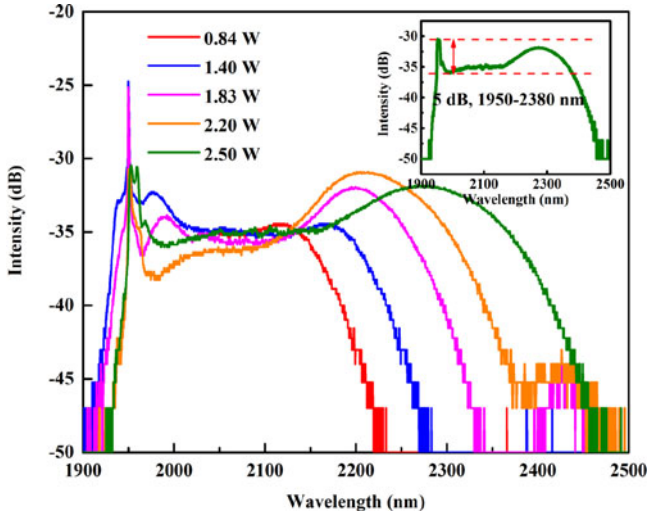

Fig. 7. Evolution of output spectra from the UHNA 7 fiber with different output powers. Inset: Output spectrum at the maximum output power.

long-wavelength edge is extended up to 2.46 μm. The spectrum at the maximum output power is shown in the inset of Fig. 7, which has a maximum range from 1.93 to 2.46 μm and 5 dB bandwidth of 430 nm, ranging from 1950 to 2380 nm. The power proportion beyond 2.2 μm is about 48%, which is calculated by spectral integration.

The UHNA 7 fiber has a ZDW of 2.6 μm, one can note that it is pumped in the normal dispersion region, where the four-wave mixing (FWM), modulation instability (MI) and stimulated Raman scattering (SRS) are mainly responsible for the spectral broadening [33]. For supercontinuum generated by picosecond pump pulses, the spontaneous growth of new frequency components from FMW or MI that play a central role in the initial spectral broadening process.

Fig. 8 depicts the different output powers from the TDFA and the UHNA 7 fiber. Due to the obvious spectral broadening and very high loss in the long wavelength region, both the slope efficiencies of the TDFA and UHNA 7 fiber decrease dramatically. Though longer nonlinear fiber may lead to a flatter spectrum, it can also reduce the output power of the supercontinuum. For higher output

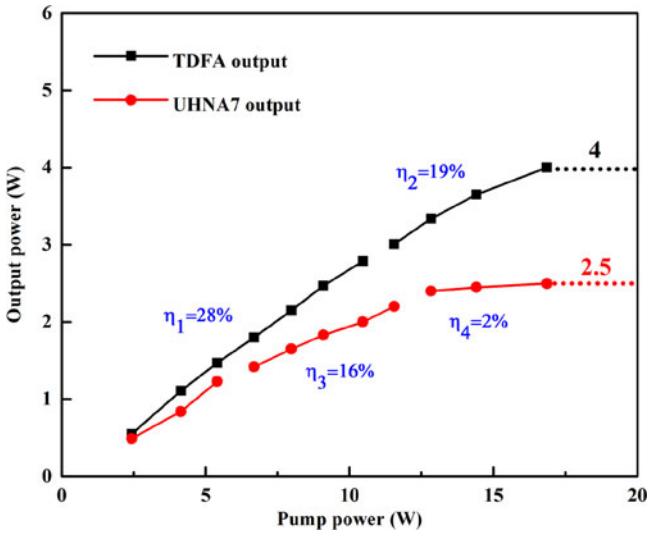

Fig. 8. Output power of the TDFA and the UHNA 7 fiber versus the incident pump power.

power and conversion efficiency, the length of the nonlinear fiber should be optimized in the future work.

Compared with the fundamental mode-locking pulse, noise-like pulse is rather than an integrated single pulse, which is actually a pulse envelope formed with fs-level inner pulses [34]. And the fs-level inner pulse of the noise-like pulse will lead to strong self-phase modulation (SPM) and SRS in the nonlinear fiber [35], [36]. The supercontinuum generation also benefits from the SPM and SRS effects.

3. Conclusion

In conclusion, we have demonstrated a SESAM based passively mode-locked TDFL with dual-operation regime, including fundamental mode-locking and noise-like twin-pulse regimes. Optical amplification characteristics of the TDFL which could operate in dual-operation regime have been demonstrated for the first time. The amplified optical signal was fed into a segment of highly Ge-doped UHNA fiber, cascaded Raman light and Supercontinuum generation were realized, respectively. The achieved total average power of two orders of Stokes Raman light is 3.75 W, centered at 2.13 and 2.35 μm, respectively. The generated supercontinuum can reach 2.5 W average power with a flat spectrum spanning from 1.93 to 2.46 μm. In our future work, we will optimize the amplification characteristics of the TDFL and focus on the interaction between ultrafast pulses and nonlinear fibers.

References

[1] G. Whitenett, G. Stewart, H. Yu, and B. Culshaw, "Investigation of a tuneable mode-locked fiber laser for application to multipoint gas spectroscopy," *J. Lightw. Technol.*, vol. 22, no. 3, pp. 813–819, Mar. 2004.
[2] S. Mehravar, R. A. Norwood, N. Peyghambarian, and K. Kieu, "Real-time dual-comb spectroscopy with a free-running bidirectionally mode-locked fiber laser," *Appl. Phys. Lett.*, vol. 108, 2016, Art. no. 231104.
[3] C. Hoy *et al.*, "Clinical ultrafast laser surgery: Recent advances and future directions," *IEEE J. Sel. Top. Quantum Electron.*, vol. 20, no. 2, Mar./Apr. 2014, Art. no. 7100814.
[4] Z. Nagy *et al.*, "Complications of femtosecond laser-assisted cataract surgery," *J. Cataract Refractive Surg.*, vol. 40, pp. 20–28, 2014.
[5] R. Kammel *et al.*, "Enhancing precision in fs-laser material processing by simultaneous spatial and temporal focusing," *Light—Sci. Appl.*, vol. 3, 2014, Art. no. e169.
[6] W. Watanabe, Y. Li, and K. Itoh, "Ultrafast laser micro-processing of transparent material," *Opt. Laser Technol.*, vol. 78, pp. 52–61, 2016.

[7] Z. Zheng *et al.*, "Scaling all-fiber mid-infrared supercontinuum up to 10 W-level based on thermal-spliced silica fiber and ZBLAN fiber," *Photon. Res.*, vol. 4, no. 4, pp. 135–139, 2016.
[8] C. Petersen *et al.*, "Mid-infrared supercontinuum covering the 1.4–13.3 μm molecular fingerprint region using ultra-high NA chalcogenide step-index fibre," *Nature Photon.*, vol. 8, pp. 830–834, 2014.
[9] Z. Sun *et al.*, "Graphene mode-locked ultrafast laser," *ACS Nano*, vol. 4, no. 2, pp. 803–810, 2010.
[10] A. Martinez and Z. Sun, "Nanotube and graphene saturable absorbers for fibre lasers," *Nature Photon.*, vol. 7, pp. 842–845, 2013.
[11] J. Tarka *et al.*, "Power scaling of an All-PM Fiber Er-Doped mode-locked laser based on graphene saturable absorber," *IEEE J. Sel. Top. Quantum Electron.*, vol. 23, no. 1, pp. 60–65, Jan./Feb. 2017.
[12] F. Wang *et al.*, "Wideband-tuneable nanotube mode-locked fiber laser," *Nature Nanotechnol.*, vol. 3, pp. 738–742, 2008.
[13] C. Castellani *et al.*, "Ultrafast Raman laser mode-locked by nanotubes," *Opt. Lett.*, vol. 36, no. 20, pp. 3996–3998, 2011.
[14] M. Chernysheva *et al.*, "Double-wall carbon nanotube hybrid mode-locker in tm-doped fibre laser: A novel mechanism for robust bound-state solitons generation," *Sci. Rep.*, vol. 7, p. 44314, 2017.
[15] C. Zhao *et al.*, "Ultra-short pulse generation by a topological insulator based saturable absorber," *Appl. Phys. Lett.*, vol. 101, p. 211106, 2012.
[16] W. Liu *et al.*, "70-fs mode-locked erbium-doped fiber laser with topological insulator," *Sci. Rep.*, vol. 6, p. 19997, 2016.
[17] J. Lee, J. Koo, and J. Lee, "A pulse-width-tunable, mode-locked fiber laser based on dissipative soliton resonance using a bulk-structured Bi2Te3 topological insulator," *Opt. Eng.*, vol. 55, no. 8, p. 081309, 2016.
[18] P. Yan *et al.*, "A practical topological insulator saturable absorber for mode-locked fiber laser," *Sci. Rep.*, vol. 5, p. 8690, 2015.
[19] Q. Wang, J. Geng, Z. Jiang, T. Luo, and S. Jiang, "Mode-locked Tm-Ho-codoped fiber laser at 2.06 μm," *IEEE Photon. Technol. Lett.*, vol. 23, no. 11, pp. 682–684, Jun. 2011.
[20] S. Liu *et al.*, "Switchable SP dual-wavelength mode-locked TDFL incorporating a PM-FBG and SESAM," *IEEE Photon. Technol. Lett.*, vol. 29, no. 6, pp. 551–554, Mar. 2017.
[21] L. Gomes, L. Orsila, T. Jouhti, and O. Okhotnikov, "Picosecond SESAM-based ytterbium mode-locked fiber lasers," *IEEE J. Sel. Top. Quantum Electron.*, vol. 10, no. 1, pp. 129–136, Jan./Feb. 2004.
[22] S. Smirnov, S. Kobtsev, and S. Kukarin, "Efficiency of non-linear frequency conversion of double-scale pico-femtosecond pulses of passively mode-locked fiber laser," *Opt. Exp.*, vol. 22, no. 1, pp. 1058–1064, 2014.
[23] Y. Lian *et al.*, "Switchable multiwavelength fiber laser using erbium-doped twin-core fiber and nonlinear polarization rotation," *Laser Phys. Lett.*, vol. 14, p. 55101, 2017.
[24] M. Olivier, M. Gagnon, and M. Piché, "Automated mode locking in nonlinear polarization rotation fiber lasers by detection of a discontinuous jump in the polarization state," *Opt. Exp.*, vol. 23, no. 5, pp. 6738–6746, 2015.
[25] A. Komarov and K. Komarov, "Multistability and hysteresis phenomena in passive mode-locked lasers," *Phys. Rev. E*, vol. 62, no. 6, pp. 7607–7610, 2000.
[26] T. Schreiber, B. Ortac, J. Limpert, and A. Tunnermann, "On the study of pulse evolution in ultra-short pulse mode-locked fiber lasers by numerical simulations," *Opt. Exp.*, vol. 15, no. 13, pp. 8252–8262, 2007.
[27] Q. Wang, T. Chen, B. Zhang, A. Heberle, and K. Chen, "All-fiber passively mode-locked thulium-doped fiber ring oscillator operated at solitary and noiselike modes," *Opt. Lett.*, vol. 36, no. 19, pp. 3750–3752, 2011.
[28] J. Li *et al.*, "All-fiber passively mode-locked Tm-doped NOLM-based oscillator operating at 2-μm in both soliton and noisy-pulse regimes," *Opt. Exp.*, vol. 22, no. 7, pp. 7875–7882, 2014.
[29] G. Sobon, J. Sotor, T. Martynkien, and K. Abramski, "Ultra-broadband dissipative soliton and noise-like pulse generation from a normal dispersion mode-locked Tm-doped all-fiber laser," *Opt. Exp.*, vol. 24, no. 6, pp. 6156–6161, 2016.
[30] Y. Kwon, L. Vazquez-Zuniga, S. Lee, H. Kim, and Y. Jeong, "Numerical study on multi-pulse dynamics and shot-to-shot coherence property in quasi-mode-locked regimes of a highly-pumped anomalous dispersion fiber ring cavity," *Opt. Exp.*, vol. 25, no. 4, pp. 4456–4469, 2017.
[31] H. Jiang, L. Zhang, and Y. Feng, "Silica-based fiber Raman laser at $>$2.4 μm," *Opt. Lett.*, vol. 40, no. 14, pp. 3249–3252, 2015.
[32] K. Yin, B. Zhang, J. Yao, L. Yang, L. Li, and J. Hou, "High-peak-power picosecond fiber laser at 2050 nm and its application to cascaded Raman light $>$2 μm," *IEEE Photon. Technol. Lett.*, vol. 28, no. 10, pp. 1119–1122, May 2016.
[33] P. Yan *et al.*, "Double cladding seven-core photonics crystal fibers with different GVD properties and fundamental supermode output," *J. Lightw. Technol.*, vol. 31, no. 23, pp. 3658–3662, Dec. 2013.
[34] H. Chen, S. Chen, Z. Jiang, and J. Hou, "0.4 μJ, 7 kW ultrabroadband noise-like pulse direct generation from an all-fiber dumbbell-shaped laser," *Opt. Lett.*, vol. 40, no. 23, pp. 5490–5493, 2015.
[35] A. Zaytsev, C. Lin, Y. You, C. Chung, C. Wang, and C. Pan, "Supercontinuum generation by noise-like pulses transmitted through normally dispersive standard single-mode fibers," *Opt. Exp.*, vol. 21, no. 13, pp. 16056–16062, 2013.
[36] H. Chen, X. Zhou, S. Chen, Z. Jiang, and J. Hou, "Ultra-compact Watt-level flat supercontinuum source pumped by noise-like pulse from an all-fiber oscillator," *Opt. Exp.*, vol. 23, no. 26, pp. 32909–32916, 2015.